International Journal of Biological Macromolecules

Structural insights and aggregation propensity of a super-stable MNEI mutant: a new potential building block for protein-based nanostructured materials

--Manuscript Draft--

Manuscript Number:	
Article Type:	Research Paper
Section/Category:	Proteins and Nucleic acids
Keywords:	protein fibrillar aggregation; functional amyloids; protein biomaterials.
Corresponding Author:	Delia Picone Napoli, Italy
First Author:	Rosanna Lucignano
Order of Authors:	Rosanna Lucignano
	Roberta Spadaccini
	Antonello Merlino
	Giarita Ferraro
	Delia Picone
Abstract:	Protein fibrillation is commonly associated with pathologic amyloidosis. However, several proteins can form fibrillar structures in vitro that with interesting biotechnological applications. MNEI and its variants are useful models to study the mechanism of the aggregation process governing protein fibrils formation. In this work, we have drawn attention to a MNEI derivative dubbed Mut9, already characterized as a “super stable mutant”. Comparative X-ray analysis revealed the structural grounds of the higher stability of Mut9 with respect to MNEI. Despite the close similarity of the structures, inspection of each mutation revealed how the substitutions eliminate several unfavorable interactions and stabilize the Mut9 structure. Molecular dynamic predictions confirmed the presence of a hydrogen-bonds network in Mut9 which increases its stability, in particular at neutral pH. Thioflavin-T binding assays indicated that the aggregation process occurs both at acidic and neutral pH, with and without addition of NaCl, even if with a different kinetics. Transmission Electron Microscopy showed a fibrillar organization of the aggregates in all the tested conditions, albeit with some differences in the quantity and in the morphology of the fibrils. Our data underline the great potential of Mut9, which combines great stability in solution with the versatile conversion into nanostructured biomaterials.
Suggested Reviewers:	Raffaele Mezzenga raffaele.mezzenga@hest.ethz.ch Expertise: Fundamental understanding of self-assembly processes inf protein fibrillation process
	Douglas V. Laurents dlaurents@iqfr.csic.es Expertise: Study of protein folding and stability; Study of proteins involved in harmful amyloid states
	Simona Tomaselli simona.tomaselli@scitec.cnr.it Expertise: Structural studies of amyloid peptides, kinetics and mechanism of aggregation
Opposed Reviewers:	

UNIVERSITÀ DEGLI STUDI DI NAPOLI FEDERICO II
SCUOLA POLITECNICA E DELLE SCIENZE DI BASE

DIPARTIMENTO DI SCIENZE CHIMICHE

Dear Editor,

enclosed please find the article entitled "Structural insights and aggregation propensity of a super-stable MNEI mutant: a new potential building block for protein-based nanostructured materials" by R. Lucignano, R. Spadaccini, A. Merlino, G. Ferraro, D. Picone, which we would like to submit to *International Journal of Biological Macromolecules*, as a research article. The reasons that induced us to submit this manuscript to *International Journal of Biological Macromolecules* are summarised below.

The paper we propose for publication reports a comparative analysis from the structural point of view of two proteins: MNEI, a single chain derivative of the sweet plant protein monellin, and its mutant dubbed Mut9.

We focused the attention on this mutant, already characterized as "super stable" and "super sweet", due to the presence of point substitutions which provide interesting properties to the protein. X-ray studies revealed the network of interactions responsible for the higher stability of Mut9 with respect to MNEI, despite the close similarity of their structures. As MNEI is also a useful model for amyloid aggregation studies, in this paper we have compared the aggregation tendency of the two proteins. Molecular dynamic simulations showed a similar behaviour of the two proteins at acidic pH, while highlighted a superior stability of the structure of Mut9 at neutral pH. This difference in our opinion can be related to the capability of Mut9 to form fibrils both at acidic and neutral pHs, while MNEI can form fibrillar structures only at pH 2.5, giving rise to amorphous aggregates at pH 6.8.

The results we report in this manuscript put on a structural basis the different aggregation behaviour of the two proteins and suggest that, despite the close similarity with MNEI, Mut9 is not only a better candidate as sugar substitute, but also a more versatile building block to design protein based nanostructured materials.

Looking forward to hearing for your judgment.

Our best regards,

Delia Picone and Giarita Ferraro

Abstract

Protein fibrillation is commonly associated with pathologic amyloidosis. However, under appropriate conditions several proteins form fibrillar structures *in vitro* that can be used for biotechnological applications. An example is represented by MNEI and its variants, useful models to study the molecular basis of the aggregation process which governs protein fibrils formation. In this work, we have drawn attention to a MNEI mutant dubbed Mut9, which was already characterized as a "super stable mutant". Comparative X-ray analysis revealed the structural grounds of the higher stability of Mut9 with respect to MNEI. Despite the close similarity of the structures, inspection of each mutation one by one highlighted how the substitutions eliminate several unfavorable interactions and have a stabilizing effect on Mut9 global structure. Molecular dynamic predictions confirmed the presence of a hydrogen-bonds network in Mut9 which increases its stability, in particular at neutral pH. Thioflavin-T (ThT) binding assays indicated that the aggregation process occurs both at acidic and neutral pH, with and without addition of NaCl, even if with a different kinetic. Accordingly, Transmission Electron Microscopy (TEM) showed a fibrillar organization of the aggregates in all the tested conditions, albeit with some differences in the quantity and in the morphology of the fibrils. Our data underline the great potential of Mut9, which combines great stability in solution with the versatile conversion into nanostructured biomaterials.

- MNEI and its variants are useful models for protein fibrillary aggregation process studies.
- Mut9 was designed as a super-stable and super-sweet MNEI mutant.
- X-ray and MD studies highlighted the higher stability of Mut9 at neutral pH.
- Differently from MNEI, Mut9 can form fibrils both at acidic and neutral pH.
- Mut9 has a great potential as building-block to design nanostructured biomaterials.

Graphical abstract

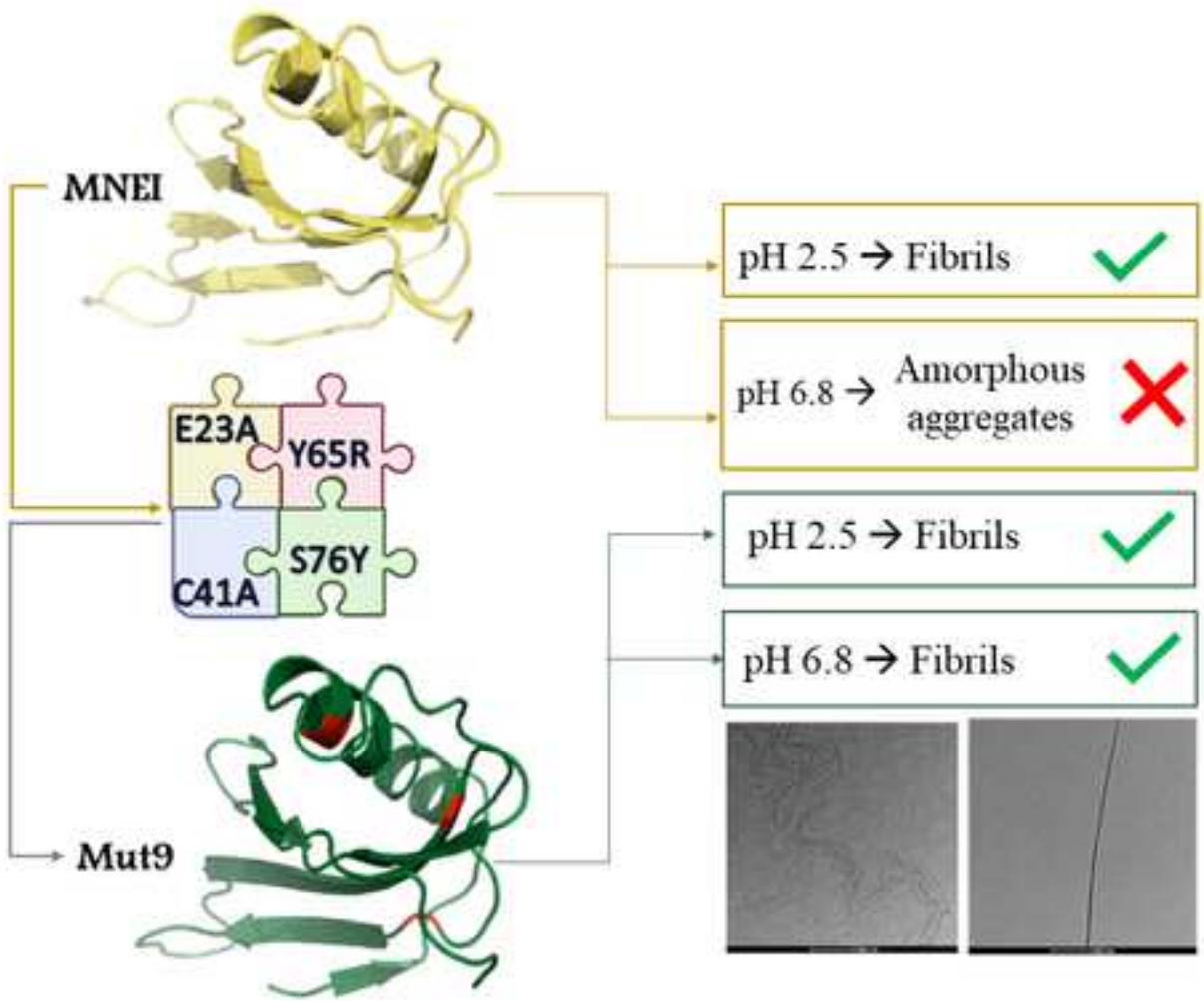

Structural insights and aggregation propensity of a super-stable MNEI mutant: a new potential building block for protein-based nanostructured materials

Rosanna Lucignano[a], Roberta Spadaccini[b], Antonello Merlino[a], Giarita Ferraro[a]*, Delia Picone[a]*

[a] Department of Chemical Sciences, University of Naples Federico II, Complesso Universitario di Monte Sant'Angelo, Via Cintia, 80126, Napoli, Italy

[b] Department of Science and Technology, University of Sannio, Via de Sanctis, 82100, Benevento, Italy

*** Corresponding Authors**

Prof. Delia Picone - Department of Chemical Sciences, University of Naples Federico II, Complesso Universitario di Monte Sant'Angelo, via Cintia, 21, 80126, Naples, Italy - Phone number: +39 081-2539332 081-674406 - email: picone@unina.it;

Dr. Giarita Ferraro - Department of Chemical Sciences, University of Naples Federico II, Complesso Universitario di Monte Sant'Angelo, via Cintia, 21, 80126, Naples, Italy - Phone number: +39 081-674269 - email: giarita.ferraro@unina.it

Abstract

Protein fibrillation is commonly associated with pathologic amyloidosis. However, under appropriate conditions several proteins form fibrillar structures *in vitro* that can be used for biotechnological applications. An example is represented by MNEI and its variants, useful models to study the molecular basis of the aggregation process which governs protein fibrils formation. In this work, we have drawn attention to a MNEI derivative dubbed Mut9, which was already characterized as a "super stable mutant". Comparative X-ray analysis revealed the structural grounds of the higher stability of Mut9 with respect to MNEI. Despite the close similarity of the structures, inspection of each mutation one by one highlighted how the substitutions eliminate several unfavorable interactions and have a stabilizing effect on Mut9 global structure. Molecular dynamic predictions confirmed the presence of a hydrogen-bonds network in Mut9 which increases its stability, in particular at neutral pH. Thioflavin-T (ThT) binding assays indicated that the aggregation process occurs both at acidic and neutral pH, with and without addition of NaCl, even if with a different kinetics. Accordingly, Transmission Electron Microscopy (TEM) showed a fibrillar organization of the aggregates in all the tested conditions, albeit with some differences in the quantity and in the morphology of the fibrils. Our data underline the great potential of Mut9, which combines great stability in solution with the versatile conversion into nanostructured biomaterials.

Keywords: protein aggregation; functional amyloids; MNEI; Mut9; X-ray structure; protein fibrils; nanostructured biomaterial.

1.1 Introduction

The protein fibrillation mechanism has been often[1] studied with reference to several human diseases that are characterized by the formation of amyloid deposits[2,3]. However, it has been widely demonstrated that a huge number of proteins, unrelated to any known disease, can form amyloid structures *in vitro* under appropriate conditions[4]. In fact, self-assembling proteins became popular not only for their implication in pathological conditions, but also for their potential as building blocks to obtain protein-based nanomaterials with attracting potential applications, such as targeted drug delivery systems for cancer therapy or diagnostic tools or vaccine development[5]. Protein-based nanomaterials present several advantages, such as sustainable and scalable production, long-term stability, and absence of immunogenicity[6,7].

The ability of proteins to self-assemble forming fibrils is an intricate process and is influenced by different parameters, intrinsic or extrinsic to the protein. Extrinsic factors include physico-chemical parameters, such as pH, temperature, ionic strength and protein concentration[8–10], while the intrinsic factors refer to the specific features of the protein, such as charge, hydrophobicity, patterns of polar and non-polar residues, and also propensity to adopt different secondary structure motifs. In a globular protein the polypeptide main chain and the hydrophobic side chains are largely buried within the folded structure. When they become exposed, for example when the protein is partly unfolded, the conversion of protein molecules into aggregated structures has a higher probability to occur[11]. The fibrillation is generally characterized by a lag phase, followed by a period of rapid growth, and seems to involve the formation of soluble oligomers[12,13].

Specific regions of the protein, known as aggregation-prone regions, may have a central role in the formation of stable fibrillar aggregates[14,15]. The identification of such regions could drive the design of protein mutants able to form ordered intermolecular assemblies that can be easily isolated, replicated and used for potential biotechnological applications.

In this framework we have undertaken an investigation of the aggregation process of MNEI, a sweet, single chain derivative of the small plant protein monellin designed to be sweeter and more stable compared to the parent one[16]. Besides its potential as protein-based sweetener, this globular protein also represents a good model for protein self-assembly studies. Indeed, the folding and unfolding processes of MNEI have been deeply characterized[17–19] and appear to be multistate, with parallel pathways populated by multiple intermediates[18]. Jha and coworkers[20] demonstrated that MNEI unfolding process initiates with the protein expansion into a dry molten globular state in which the single α-helix moves out from the native state gradually[20]. It has been recently reported a systematic study of the aggregation mechanisms of this protein showing that MNEI, under mild denaturing conditions/early unfolding stages, can be converted into insoluble, amyloid state, giving rice to linear or branched structures. All these structures can be observed at acidic pH (pH = 2.5), where the prolonged incubation of the protein, at a temperature below its melting temperature, prompts the formation of aggregates with the typical features of amyloid fibrils. On the contrary, at neutral pH (pH = 6.8), only amorphous aggregates can be detected[21], suggesting that pH is the main switch between amyloid and amorphous aggregation[22]. Furthermore, the presence of salts, particularly chlorides, accelerates fibrils formation[23]. Due to its great potential, many studies have been conducted to improve MNEI features. Indeed, site-directed mutagenesis has been used as a tool for the rational design of mutants with greater resistance and higher thermal and chemical stability, even at neutral pH. Liu and co-workers pointed out that many mutants, able to enhance the thermostability of the protein, were distributed at the two ends of α-helix[24]. They showed how the replacement of the unpartnered ionizable residue Glu23 from the hydrophobic core of the protein with an alanine (E23A) can stabilize the native state of the protein. In addition, they proved that C41 residue, located at the second β-strand, can contribute to thermostability improvement playing a concerted role with E23 to account for the pH-dependent stability of the protein at pH > 8[24]. Esposito *et al.* designed and produced Y65R-MNEI, a mutant significantly sweeter than the parent protein, predicted to interact more efficiently

with the sweet receptor T1R2:T1R3[25], while keeping the same aggregation propensity of MNEI[21].

Based on these findings, recently we have designed a new mutant, Mut9, selecting the most promising point mutations: Y65R, E23A, C41A and S76Y[26]. Mut9 showed high stability in acidic and neutral environments, a higher melting temperature (over 20 °C) than that of MNEI and resulted twice sweeter than MNEI. Notably, it preserved its structure and function even after 10 minutes boiling, particularly at pH 6.8, and after 6-months of shelf-life in different conditions. This protein is the proof that multiple mutations of different residues can lead to an additive performance with both improved sweetness and stability, suggesting that the sweetness and stability could be modulated by the independent molecular mechanism.

Inspired by these features, in this paper we have addressed a comparative study between MNEI and Mut9 to understand the structural grounds of the higher stability of the latter protein and investigate its amyloid aggregation propensity. The analysis of the effect of single point mutations on Mut9 stability has been evaluated by means of X-ray crystallography coupled to molecular dynamic predictions. In addition, we have evaluated Mut9 aggregation tendency at two different pHs and compared the morphology of the obtained fibrils. Specifically, we have studied the kinetic of aggregation, in different experimental conditions, by using a ThT assay, and analyzed fibrils morphology by TEM.

1.2 Results

1.2.1 X-ray structures of MNEI and Mut9

The structures of MNEI and Mut9 from isomorphic crystals possess 2032 and 1976 atoms, respectively. The X-ray structures (Fig. 1), obtained from crystals with two molecules in the

asymmetric unit (chain A and chain B), have been refined at a resolution of 1.19 and 1.50 Å, and to R-factor and Rfree values within the range 0.218/0.256 and 0.223/0.274, respectively.

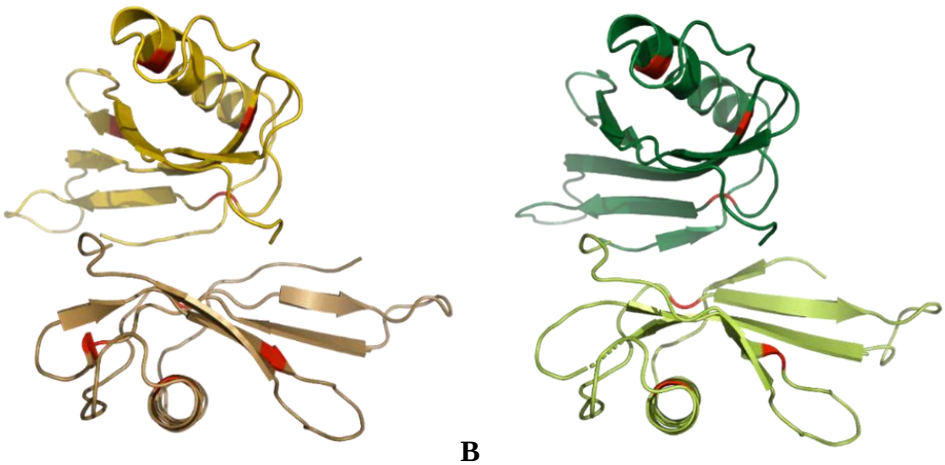

A **B**

Fig. 1. Cartoon representation of the X-ray structures of MNEI (A) and Mut9 (B). The two molecules of the asymmetric unit are shown in dark yellow and gold for MNEI and in light and dark green for Mut9. The position of the mutated residues is indicated in red.

Both structures are very similar to each other, as revealed by the analysis of the values of the root mean square deviations of the distances between the Cα (RMSD, Table S1), and to the structures of MNEI and its mutants reported in literature (Table S2). In fact, the graphs of B-relative (obtained by normalization of B-factors[27] reported as a function of residue of MNEI and Mut9 (Fig. S1) are very similar, except for the region between residues 45-60, where Mut9 shows higher B-relative values than MNEI. This difference could be related to the L23 loop located in this region (residues 47-56) which, in all the structures reported for MNEI and its derivatives, is generally highly flexible or disordered. Indeed, in the structure of Mut9 the electron density map in this region is not well defined.

To understand the determinants of the different thermal stability of MNEI and Mut9, the structural features of each molecule of the asymmetric unit were analyzed and compared. MNEI and Mut9

possess a comparable number of hydrogen bonds and salt bridges, similar solvent-accessible surfaces and hidden regions, and similar volume (Table S3). Thus, the two proteins show similar structural features, suggesting that the presence of the mutation sites do not introduce variations of general protein conformation, as also suggested by their capability to recognize the same receptors, eliciting the sweet taste. Therefore, we have analyzed one by one the single point mutations to investigate the reasons for the increased Mut9 stability with respect to MNEI.

1.2.2 Analysis of the effects of single point mutations

Y65R mutation. The mutation Y65R introduces a positive charge on the surface of MNEI associated with a sweetness increase[28] and a thermal stability decrease of the protein[21]. Crystallographic studies revealed that the mutation induces structural changes in the C-terminal region of the protein, responsible for the lower stability of Y65R mutant to the respect of MNEI[21]. In particular, the Arg65 side chain in Y65R mutant appears disordered. The disorder of this residue affects the conformation of the residue Tyr63, which, in the structure of MNEI, interacts with the residue Phe94 at the C-terminus. Consequently, in the Y65R mutant, the distances between Tyr63 and Phe94 are slightly greater than those observed in MNEI[21]. This difference could contribute to the lower thermal stability of the mutant compared to that of MNEI. In contrast, in the two chains of the asymmetric unit of MNEI and Mut9, the electron density map of residue 65 is well defined (Fig. S2). The analysis of the distances between residues 63 and 94 shows that the neighborhood of residue 65 in Mut9 is more similar to MNEI than to Y65R, suggesting that in this mutant the Y65R mutation is less destabilizing than in Y65R-MNEI (Table S4, Fig. 2).

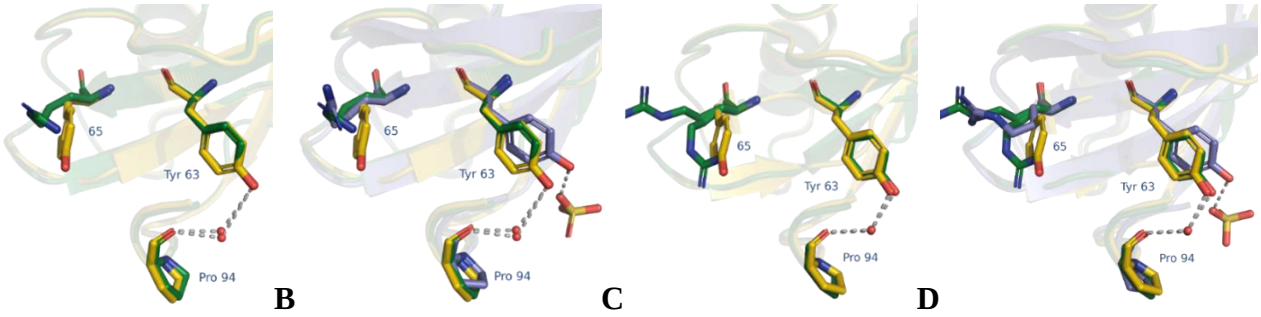

Fig. 2. Neighborhood of residue 65. The interactions of residues 63 and 94, which have been hypothesized to play an important role in protein stability, are highlighted. In yellow MNEI, in green Mut9 and in blue Y65R. Chains A in panels A and B, chains B in panels C and D.

C41A mutation. The C41A mutation is related to the sweetness decrease and the thermal stability increase of MNEI[24]. This residue is located in a hydrophobic pocket formed by residues Ile6, Thr12, Leu15, Val37 and Leu62. In both molecules of the asymmetric unit of MNEI crystals, the sulfur atom of Cys41 forms unfavorable interactions with the residues of this pocket. In Mut9 the C41A substitution eliminates the unfavorable MNEI-Cys41 interactions, thus stabilizing the structure of the mutant. In fact, the side chain of the alanine is less bulky than that of cysteine. In this way the surrounding residues have much more space. The comparison between the structures of MNEI and Mut9 also shows a conformational change of Leu62 side chain due to the mutation. Leu62 occupies part of the empty space introduced by the C→A substitution (Fig. 3).

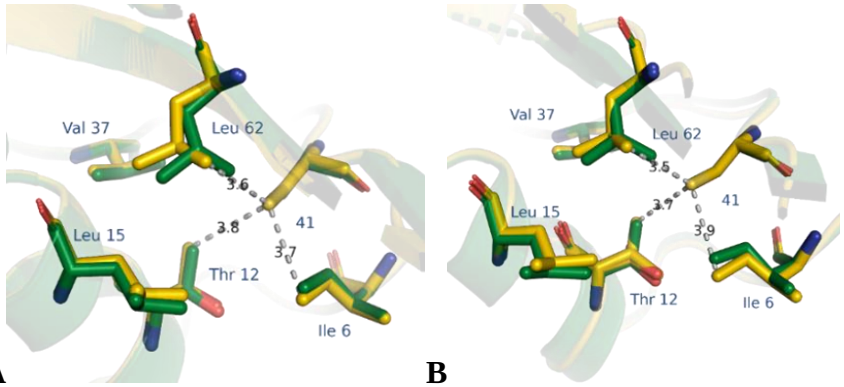

Fig. 3. Details of the interactions of residue 41 with the surrounding residues in the structures of MNEI (yellow) and Mut9 (green). Chains A are reported in panel A, chains B in panel B. The distances are represented by grey dashes.

This conformational variation is observed in both molecules of the asymmetric unit. In the two chains of the asymmetric unit of MNEI and Mut9, the electron density map of residue 41 is well defined (Fig. S3). Details of the distances between residues 41 and 62 are reported in Table S5.

E23A mutation. The E23A mutation is related to a strong increase in thermal stability[29]. pH plays an important role in modulating the stability of MNEI and its mutants. It has been demonstrated that residue E23, buried in a hydrophobic pocket of the protein at one end of the alpha helix, is responsible for a pH dependent stability of the protein, due to its anomalous pKa. In the two chains of the asymmetric unit of MNEI and Mut9, the electron density map of residue 23 is well defined (Fig. S4). MNEI structure, notably, shows that the Glu23 side chain is in contact with the residues Ile26, Phe89, Leu86, Tyr29 e Gln28 (Fig. 4) in both molecules of the asymmetric unit, but these interactions are energetically unfavorable. The substitution E23A in Mut9 removes these unfavorable interactions and introduces an empty space around residue 23, which is partly occupied by small displacements of the residues of the hydrophobic pocket.

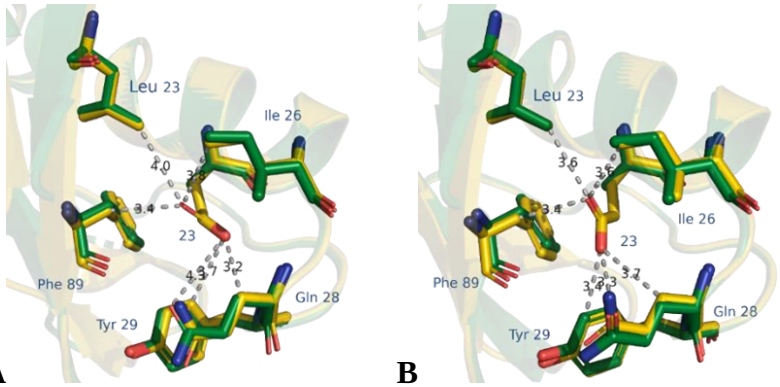

A **B**

Fig. 4. Details of the interactions of residue 23 with the surrounding residues in the structures of MNEI (yellow) and Mut9 (green). Chains A are reported in panel A, chains B in panel B. The distances are represented by grey dashes.

The comparison of the distances between Phe89 and A/Glu23 residues are reported in Table S6. This could contribute to the increased stability of Mut9 with respect to MNEI.

S76Y mutation. Residue 76 is located within the β3 sheet of the protein. Literature results demonstrate that replacing Ser76 with Tyr increases the stability of the protein[30]. Residue 76 is well defined in the electron density maps of MNEI and Mut9 (Fig. S5). In the two molecules of MNEI structure, serine forms an unfavorable interaction with the Lys85 atoms and a hydrogen bond with a water molecule (Fig. 5). In the Mut9 structure, the tyrosine side chain forms a hydrogen bond with the carbonyl oxygen of Lys56 and with the side chain of Asp78, although in one of the two molecules of the asymmetric unit this interaction is mediated by the presence of a water molecule (Fig. 5). Tyr76 side chain forms van der Waals interactions with carbon atoms of the residues Ile46, Lys56, Lys85 and Leu87, which are in its neighborhood. All these interactions can make an important contribution in increasing the stability of the mutant with respect to MNEI.

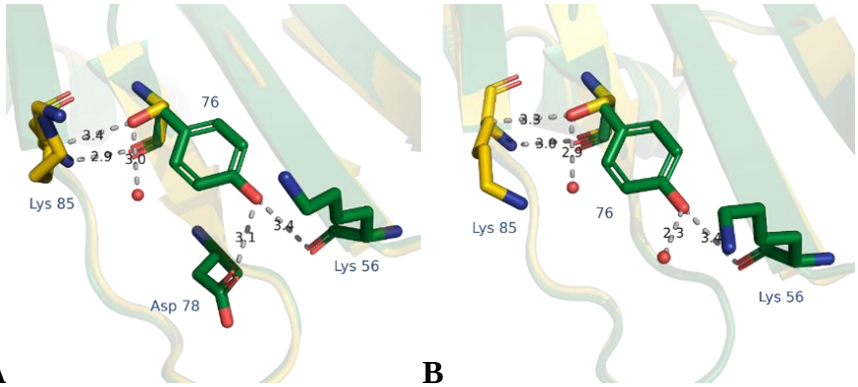

A **B**

Fig. 5. Details of the interactions of residue 76 with the surrounding residues in the structures of MNEI (yellow) and Mut9 (green). Chains A are reported in panel A, chains B in panel B. The distances are represented by grey dashes.

The punctual analysis of the additional interactions in Mut9 accounts for the increased thermal stability observed for the protein with respect to the parent MNEI both at acidic and neutral pH[26]. Indeed, the network of stabilizing interactions located in different protein areas counteracts the 4-8 degrees decrease of the melting temperature associated to the mutation Y65R[21], due to the increased distances between residues Tyr63 and Phe94.

1.2.3 Aggregation propensity

The aggregation tendency of Mut9 was studied by standard ThT fluorescence assay and compared with literature data reported for MNEI[21]. The protein was incubated, with and without NaCl, at pH 2.5 and 6.8, at 75 and 90 °C, respectively, *i.e.*, in temperature conditions corresponding to the early unfolding steps, according to the thermal denaturation study previously reported[26]. Indeed, it has been shown that partial protein unfolding is a preliminary step in the formation of amyloid-like protein fibrils[31]. The aggregation kinetics was followed for two days, for pH 6.8, and for four days, for pH 2.5, monitoring the ThT fluorescence signal until a stationary phase was reached (Fig.

6A). The data reported in Fig. 6 indicated that ThT fluorescence intensity increases as function of time for all the analyzed samples, but the pH drastically influences ThT binding. Particularly, i) at neutral pH, the signal reached the plateau after only one day of incubation, and the intensity is lower in comparison with the one obtained at acidic pH; ii) at pH 2.5, the *plateau* was reached after two days of incubation. The curves from all the samples show a sigmoidal line-shape, more evident at acidic pH, as expected for amyloid fibrils formation mechanism, which involves three phases, i.e., lag, elongation, and *plateau*[31]. Interestingly, at both pHs, the aggregation process occurs also without NaCl. Nevertheless, the ionic strength affects the kinetic in an opposite way in these two conditions. In fact, at acidic pH the kinetic in the presence of NaCl is faster than that in the absence of NaCl, while, at neutral pH, the ionic strength delays the kinetics. Anyway, quite a high response to ThT assay, under all conditions, suggests the possible presence of fibrillar aggregates. To investigate the morphology of the aggregates formed by Mut9, aliquots of the samples incubated for two days at neutral pH and for four days at acidic pH were analyzed by electron transmission microscopy (TEM). Representative images of the samples obtained under all conditions tested are reported in Fig. 6 (from B to E). Differently from MNEI, Mut9 aggregates showed a fibrillar organization at both acidic and neutral pH, independently on the presence of NaCl. However, the quantity and the morphology of the fibrils are influenced by NaCl at both pHs, reflecting the different ThT fluorescence intensity. In fact, at pH 2.5, in the presence of NaCl the ThT emission is much more intense, suggesting the presence of a higher number of β-structures constituting the amyloid fibrils. This hypothesis is confirmed by TEM. In fact, as observed in Fig. 6 C, there are more fibrils, and they are more branched in comparison to the fibrils of the sample without salt (Fig. 6 B). On average, the fibrils formed in the presence of sodium chloride have a diameter of 23 ± 2 nm or, if branched, of 14 ± 1 nm, while in the absence of salt show a width of 21 ± 1 nm. In both cases, *i.e.*, in the absence or in the presence of NaCl, the length of fibrils is about 4 ± 1 μm. On the other hand, at pH 6.8, in the absence and in the presence of NaCl only few, very long fibrils, can be detected. In fact, as suggested by ThT binding assays, the fluorescence intensity is much lower than

that observed at acidic pH. Moreover, on the contrary of what occurs at pH 2.5, in this case the fluorescence intensity in the absence of NaCl is slightly higher than in presence of salt, and the fibrils are more branched than those obtained in the presence of NaCl (Fig.s 6 D-E).

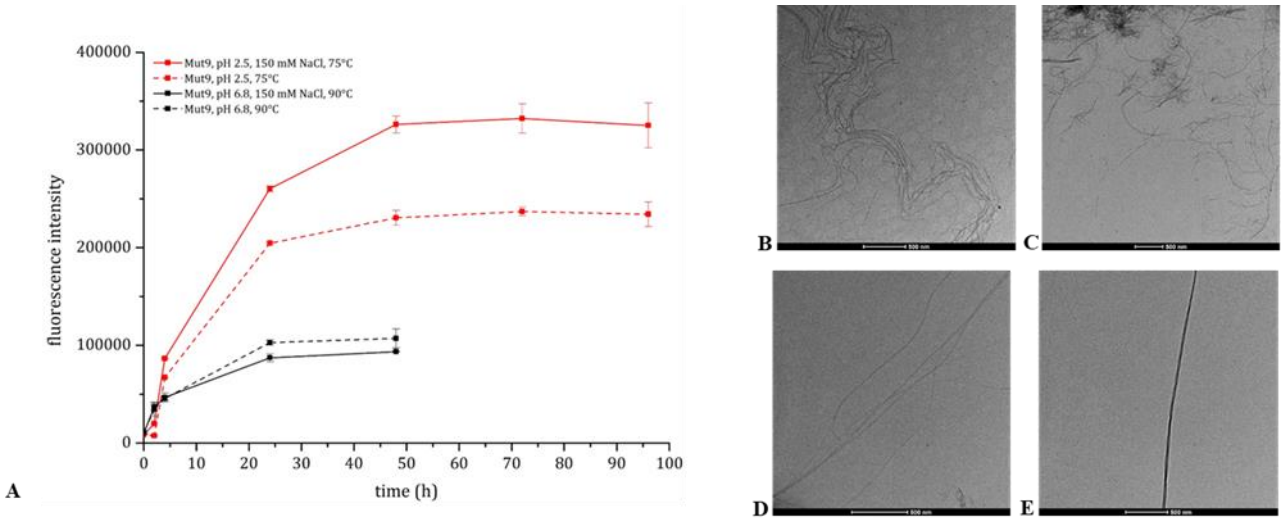

Fig. 6. ThT binding assay of Mut9 (panel A). Fluorescence intensity values are reported as function of time for: Mut9, pH 2.5, NaCl, 75 °C (solid red line), Mut9, pH 2.5, 75 °C (dotted red line), Mut9, pH 6.8, NaCl, 90 °C (solid black line) and Mut9, pH 6.8, 90 °C (dotted black line). Transmission electron images of Mut9 (panels B-E). Samples incubated in 20 mM phosphate buffer pH 2.5 at 75 °C after 96 h without (B) and with (C) 150 mM sodium chloride, and in 20 mM phosphate buffer pH 6.8 at 90 °C after 48 h without (D) and with (E) 150 mM of sodium chloride. The samples were observed without any staining procedure; therefore, protein fibrils appear darker with respect to the background. The scale bars are 500 nm.

Regarding fibrils dimensions, in both the analyzed cases there is a coexistence of fibrils formed by a single filament (13 ± 2 nm) and fibrils formed by two filaments (23 ± 1 nm). Also in these experimental conditions, the obtained fibrils show a length of about 3 ± 1 μm.

1.2.4 Molecular Dynamics

Molecular Dynamics simulations were performed on MNEI and Mut9 at acidic and neutral pH both at 300 and 350 K, to gain insights on the different behaviour of the two proteins in terms of stability and aggregation propensity (Fig. 7).

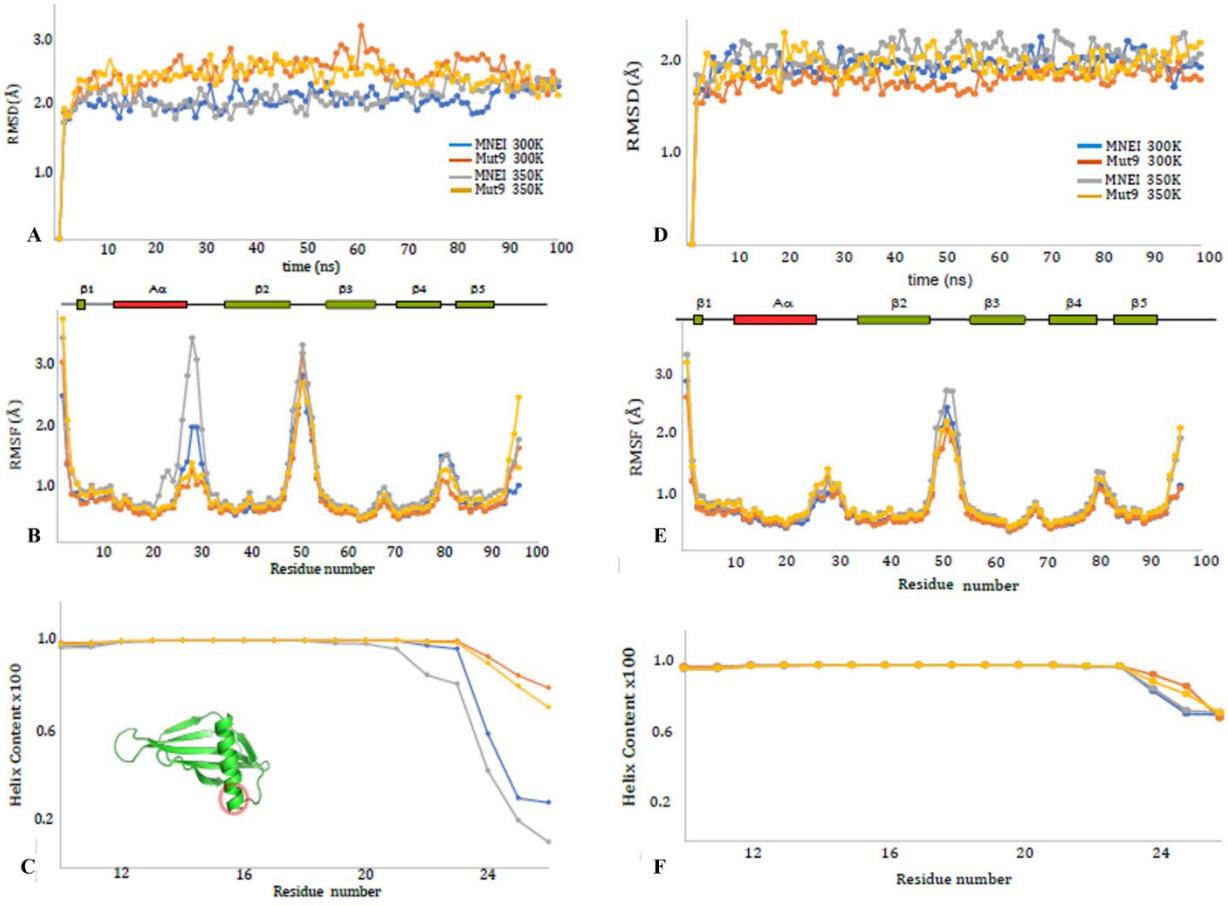

Fig. 7. Molecular dynamics simulations of MNEI and Mut9 at pH 6.8 (panels A-C) and pH 2.5 (panels D-F). RMSD along the trajectory are reported in panels A and D, while RMSF of all the Cα atoms in panels B and D, both collected at 300 K (in blue MNEI and in red Mut9) and at 350 K (in grey MNEI and in orange Mut9). In panels C and F, helical structure variation along the trajectory versus residue number are shown at pH 6.8 and pH 2.5. The region that loses the helical structure during the 100 ns trajectory is highlighted with a red circle on MNEI structure in panel C.

All MD simulations were performed at 100 ns. The structures of the two proteins stay stable along all the trajectories as shown from the root mean square deviation (RMSD) data at pH 6.8 and 2.5 (Fig.s 7A and 7D). The Cα root-mean square fluctuations (RMSF) of all residues are shown in Fig.s 7B and 7E. At acidic pH the two proteins show a similar behaviour along the trajectory (Fig. 7E); they show the same flexibility at the N and C terminus at the linker loop and the Lα2 loop, the loop connecting the C terminal region of the helix and β2 strand, as well in the region between L45 and the beginning of β5. It is interesting to note that Lα2 loop and β5 strand have been previously indicated as likely hot spots involved in triggering amyloid aggregation[32].

At pH 6.8 (Fig. 7B), MNEI is more flexible than Mut9 in the region of the Lα2 loop and the L45 loop beginning of 5β. From the analysis of the variation of secondary structure during the trajectories, MNEI at the same pH loses more that 50% of the secondary structure in the C terminal region at 300 and 350 K whereas Mut9 secondary structure is unaffected by the variation of pH and temperature (Fig.s 7C and 7F).

1.3 Discussion

MNEI and its variants are useful and established models to study the structural determinants of proteins sweetness. However, these proteins can be also studied to better understand the molecular basis of the aggregation process which governs protein fibrils formation. In the present work, we have focused the attention on two proteins of this family, MNEI and its mutant Mut9. We have already reported, in a previous work, that Mut9 is a super stable mutant[26], and even sweeter than the parent protein. Here, we showed that MNEI and Mut9 possess a comparable number of hydrogen bonds and salt bridges, similar solvent-accessible surfaces and hidden regions, and similar volume. All these features explain why the two proteins are able to interact with the same receptor, eliciting the sweet taste typical of monellin and its derivatives[26]. Furthermore, by analyzing one

by one the mutation sites, we understood why the Y65R substitution in Mut9, responsible of the increased protein sweetness, has a less destabilizing effect than that observed in the Y65R mutant[21], since the chemical environment of the mutant is more similar to that of MNEI than to that of Y65R. In addition, the E23A and C41A mutations introduce non-polar side chains into two hydrophobic pockets of the protein and eliminate a number of unfavorable interactions observed in MNEI. This procedure is known to stabilize the native structure of proteins by preventing their denaturation. Furthermore, the S76Y mutation allows the formation of hydrogen bonds and van der Waals interactions between tyrosine and the surrounding residues, in particular the formation of hydrogen bonds with residues Lys56 and Asp76. All these interactions contribute to the increase of the thermal stability of Mut9 compared to MNEI.

Mut9 can also be converted into fibrillar aggregates both at acidic and neutral pH, independently from the presence of NaCl. However, the ionic strength influences the kinetics of aggregation in a different way for the two pH conditions. At pH 2.5 and with NaCl, the kinetic is faster, while, at neutral pH, the ionic strength delays the process. The effect of salts on protein conformational stability and amyloid formation has been debated in the literature. Stabilization of misfolded forms has been proposed to promote protein fibrillization[33] but, in other cases, it has been shown that ions able to stabilize the protein secondary structure also promote aggregation[34,35]. Our results support the latter view. The ability of Mut9 to form fibrils has been confirmed by TEM analysis: branched and thin or thick and isolated fibrils have been observed in all the experimental conditions used in this study.

The aggregation studies show that Mut9 is able to form fibers of different morphology at acidic and neutral pH in contrast to MNEI that is able to form ordered fibers only at acidic pH. The analysis of molecular dynamics data points out that MNEI and Mut9 have similar behavior at acidic pH and the regions that in previous works[22] were indicated as possible aggregation hot spots are the one that show higher flexibility during the trajectories. On the other hand, the two proteins show different properties at neutral pH, in particular MNEI is more flexible along the trajectory than Mut9 and

tends to lose partially the helical structure. The exposure and the partial unfolding of the α-helix structure has been indicated as the trigger of protein aggregation start and may explain the different kinetic at neutral pH of the two proteins. In this condition, indeed, MNEI quickly aggregates and forms amorphous precipitates instead of ordered fibrils. For Mut9, this process occurs much more slowly favoring the fibers formation.

As shown from the comparison of the crystal structures, the introduction of mutations in Mut9 leads to a different network of hydrogen bonds that, can be hypothesized, favors the formation and improves the stability of amyloid fibrils at pH 7.0[36] in contrast to MNEI that at neutral pH does not form ordered fibers. The ability of Mut9 to form fibers of different morphology and size at different pHs makes the protein a promising candidate to prepare protein based nanomaterials[37,38].

In conclusion, in this work we have highlighted another interesting property of Mut9. Besides the extremely high sweetness and stability, it is also able to form long fibrils of different morphology and size at different pHs. Despite the close similarity with MNEI, it is not only a better candidate as sugar substitute, but also a more versatile building block to design protein based nanostructured materials.

1.4 Materials and Methods

1.4.1 Expression and purification of MNEI and Mut9

MNEI and Mut9 were expressed in *Escherichia Coli* BL21(DE3) and purified from the cell lysate by ion-exchange chromatography followed by size-exclusion chromatography as previously described[26].

1.4.2 Crystallization, X-ray diffraction data collection, structure solution and refinement

MNEI and Mut9 were crystalized at 293 K by hanging drop vapor diffusion and a reservoir solution containing 30-33% PEG4K, 0.1 M sodium acetate buffer pH 4.5 and 0.2 M ammonium sulfate mixing 1 µL protein (4.5 and 5.7 mg mL^{-1} in 5.0 mM HCl, respectively) with 1 µL mother liquor at 20 °C. Crystals grew within one week (Fig. S6). X-ray diffraction data were collected at 100 K on a Pilatus detector at XRD2 beamline of Elettra synchrotron, Trieste, Italy. Data collection statistics are reported in Table S7. Data were processed and scaled in $P12_11$ space group using AutoPROC[39]. Phase problem was solved by molecular replacement method using as starting model the structure from protein data bank (PDB) (2O9U). Refinement was carried out using Refmac-CCP4i[40] and model building using Coot[41]. Refinement statistics are reported in Table S7. Coordinates and structure factors have been deposited in the protein data bank under the accession codes 8Q0S and 8Q0R, respectively.

1.4.3 ThT binding assay

MNEI at a concentration of 216 µM was incubated in 20 mM phosphate buffer at pH 2.5, while Mut9, at the same concentration, was incubated in 20 mM phosphate buffer at pH 2.5 and 6.8 either with or without 150 mM NaCl. The aggregation kinetics was followed recording time points. Thioflavin T (ThT) stock solution of 1 mM was prepared dissolving ThT powered in 20 mM phosphate buffer pH 6.8. Samples at different time points were prepared by adding 19 µL of protein samples (final protein concentration 10 µM) and 12 µL of ThT stock solution (final concentration 30 µM) in 20 mM phosphate buffer pH 6.8 to a final volume of 400 µL. Fluorescence emission spectra were recorded on a HORIBA Fluoromax-4 in the range of 400-600 nm with scan speed of 100 nm/min, upon excitation at 440 nm. Excitation and emission slits were both set at 5 nm. Fluorescence intensity values at 485 nm emission were plotted as a function of time. The reported values represent the average of three independent experiments.

1.4.4 Transmission electron microscopy (TEM) analysis

Aliquots of the protein solution were taken and diluted 50 times with deionized water. 3 µL drops of the samples were deposited for 3 minutes on a carbon-coated copper TEM grid (200 mesh) and then, the excess fluid was drained off with filter paper and air-dried. Average fibril thickness was calculated from TEM images using IMAGE J (*ImageJ (nih.gov)*). The images were collected using a FEI TECNAI G2 S-twin apparatus operating at 120 kV (LaB_6 source).

1.4.5 Molecular dynamics simulations

Crystal structures of MNEI (8Q0S) and Mut9 (8Q0R) were used for Molecular dynamics simulations. Alle the calculations were performed with the Amber20 suite[42] using the ff14sb force field for the proteins, pKa values of ionizable residues of the two proteins were estimated by H++ at pH 2.5 and pH 7.0[43]. Each system was stepwise pre-equilibrated at 300K with 2 fs steps for 2 ns and run for further 100 ns as a pre-production step. Simulations were conducted under NPT conditions of constant temperature (300 K or 350 K) and pressure (1 atm); Berendsen thermostat was used to maintain the constant temperature. The SHAKE algorithm was employed to constrain bonds involving any hydrogen atoms. Periodic boundary conditions were employed to calculate non-bonded interactions using a 10 Å cut-off distance. The Particle Mesh Ewald (PME) method was used to calculate electrostatic interactions. Subsequent 100 ns trajectories were processed and evaluated in Jupyter Notebook using PYTRAJ and CPPTRAJ[44] and NGLview[45]. For each conditions were generated three independent simulations. The secondary structure variation was calculated using the AMBER DSSP algorithm.

Supplementary Material

Additional supporting information are provided as "Supplementary Material" Word file. Supporting information includes tables with the analysis of the structural features of MNEI and Mut9, with a comparison with literature data, details of the mutation sites and of the electron density maps from

the X-ray structures, pictures of MNEI and Mut9 crystals and a table summering data collection and refinement statistics.

Author Contributions

Rosanna Lucignano: Conceptualization; Data curation; Formal analysis; Investigation; Methodology; Software; Supervision; Validation; Visualization; Writing - review & editing. **Roberta Spadaccini:** Conceptualization; Data curation; Formal analysis; Investigation; Methodology; Software; Supervision; Validation; Visualization; Writing - review & editing. **Antonello** Conceptualization; Data curation; Investigation; Software; Supervision; Validation; Visualization; Writing - review & editing. **Giarita Ferraro:** Conceptualization; Data curation; Formal analysis; Investigation; Methodology; Project administration; Resources; Software; Supervision; Validation; Visualization; Roles/Writing - original draft; and Writing - review & editing. **Delia Picone:** Conceptualization; Data curation; Formal analysis; Investigation; Methodology; Project administration; Resources; Software; Supervision; Validation; Visualization; Roles/Writing - original draft; and Writing - review & editing.

Acknowledgments

We gratefully acknowledge the Elettra Synchrotron staff for their assistance during data collection and Miss. Antonella Giarra for her help during TEM images collection.

Conflict of interest statement

The authors declare no conflicts of interest.

Funding information

This research did not receive any specific grant from funding agencies in the public, commercial, or not-for-profit sectors.

References

[1] M. Jucker, L.C. Walker, Self-propagation of pathogenic protein aggregates in neurodegenerative diseases, Nature. 501 (2013) 45–51. https://doi.org/10.1038/nature12481.

[2] C.M. Dobson, The structural basis of protein folding and its links with human disease, Phil. Trans. R. Soc. Lond. B. 356 (2001) 133–145. https://doi.org/10.1098/rstb.2000.0758.

[3] D.J. Selkoe, Alzheimer's Disease Is a Synaptic Failure, Science. 298 (2002) 789–791. https://doi.org/10.1126/science.1074069.

[4] L.C. Serpell, M. Sunde, M.D. Benson, G.A. Tennent, M.B. Pepys, P.E. Fraser, The protofilament substructure of amyloid fibrils11Edited by F. E. Cohen, Journal of Molecular Biology. 300 (2000) 1033–1039. https://doi.org/10.1006/jmbi.2000.3908.

[5] W. Lohcharoenkal, L. Wang, Y.C. Chen, Y. Rojanasakul, Protein Nanoparticles as Drug Delivery Carriers for Cancer Therapy, BioMed Research International. 2014 (2014) 1–12. https://doi.org/10.1155/2014/180549.

[6] P.-L. Lam, W.-Y. Wong, Z. Bian, C.-H. Chui, R. Gambari, Recent advances in green nanoparticulate systems for drug delivery: efficient delivery and safety concern, Nanomedicine. 12 (2017) 357–385. https://doi.org/10.2217/nnm-2016-0305.

[7] H. Jahangirian, E. Ghasemian Lemraski, T.J. Webster, R. Rafiee-Moghaddam, Y. Abdollahi, A review of drug delivery systems based on nanotechnology and green chemistry: green nanomedicine, IJN. Volume 12 (2017) 2957–2978. https://doi.org/10.2147/IJN.S127683.

[8] J. Zurdo, J.I. Guijarro, J.L. Jiménez, H.R. Saibil, C.M. Dobson, Dependence on solution conditions of aggregation and amyloid formation by an SH3 domain, Journal of Molecular Biology. 311 (2001) 325–340. https://doi.org/10.1006/jmbi.2001.4858.

[9] Y. Su, P.-T. Chang, Acidic pH promotes the formation of toxic fibrils from β-amyloid peptide, Brain Research. 893 (2001) 287–291. https://doi.org/10.1016/S0006-8993(00)03322-9.

[10] Y. Kusumoto, A. Lomakin, D.B. Teplow, G.B. Benedek, Temperature dependence of amyloid β-protein fibrillization, Proc. Natl. Acad. Sci. U.S.A. 95 (1998) 12277–12282. https://doi.org/10.1073/pnas.95.21.12277.

[11] C.M. Dobson, Protein folding and misfolding, Nature. 426 (2003) 884–890. https://doi.org/10.1038/nature02261.

[12] B. Caughey, P.T. Lansbury, P ROTOFIBRILS , P ORES , F IBRILS, AND N EURODEGENERATION : Separating the Responsible Protein Aggregates from The Innocent Bystanders, Annu. Rev. Neurosci. 26 (2003) 267–298. https://doi.org/10.1146/annurev.neuro.26.010302.081142.

[13] G. Bitan, M.D. Kirkitadze, A. Lomakin, S.S. Vollers, G.B. Benedek, D.B. Teplow, Amyloid β-protein (Aβ) assembly: Aβ40 and Aβ42 oligomerize through distinct pathways, Proc. Natl. Acad. Sci. U.S.A. 100 (2003) 330–335. https://doi.org/10.1073/pnas.222681699.

[14] A.P. Pawar, K.F. DuBay, J. Zurdo, F. Chiti, M. Vendruscolo, C.M. Dobson, Prediction of "Aggregation-prone" and "Aggregation-susceptible" Regions in Proteins Associated with Neurodegenerative Diseases, Journal of Molecular Biology. 350 (2005) 379–392. https://doi.org/10.1016/j.jmb.2005.04.016.

[15] N.S. De Groot, I. Pallarés, F.X. Avilés, J. Vendrell, S. Ventura, Prediction of "hot spots" of aggregation in disease-linked polypeptides, BMC Struct Biol. 5 (2005) 18. https://doi.org/10.1186/1472-6807-5-18.

[16] D. Picone, P.A. Temussi, Dissimilar sweet proteins from plants: Oddities or normal components?, Plant Science. 195 (2012) 135–142. https://doi.org/10.1016/j.plantsci.2012.07.001.

[17] T. Kimura, T. Uzawa, K. Ishimori, I. Morishima, S. Takahashi, T. Konno, S. Akiyama, T. Fujisawa, Specific collapse followed by slow hydrogen-bond formation of β-sheet in the folding of single-chain monellin, Proc. Natl. Acad. Sci. U.S.A. 102 (2005) 2748–2753. https://doi.org/10.1073/pnas.0407982102.

[18] A.K. Patra, J.B. Udgaonkar, Characterization of the Folding and Unfolding Reactions of Single-Chain Monellin: Evidence for Multiple Intermediates and Competing Pathways, Biochemistry. 46 (2007) 11727–11743. https://doi.org/10.1021/bi701142a.

[19] A. Kaushik, J.B. Udgaonkar, Replacement of the Native cis Prolines by Alanine Simplifies the Complex Folding Mechanism of a Small Globular Protein by Eliminating both Fast and Slow

phases of Folding, Biophysical Journal. (2023) S0006349523005271. https://doi.org/10.1016/j.bpj.2023.08.012.

[20] S.K. Jha, J.B. Udgaonkar, Direct evidence for a dry molten globule intermediate during the unfolding of a small protein, Proc. Natl. Acad. Sci. U.S.A. 106 (2009) 12289–12294. https://doi.org/10.1073/pnas.0905744106.

[21] A. Pica, S. Leone, R. Di Girolamo, F. Donnarumma, A. Emendato, M.F. Rega, A. Merlino, D. Picone, pH driven fibrillar aggregation of the super-sweet protein Y65R-MNEI: A step-by-step structural analysis, Biochimica et Biophysica Acta (BBA) - General Subjects. 1862 (2018) 808–815. https://doi.org/10.1016/j.bbagen.2017.12.012.

[22] F. Donnarumma, S. Leone, M. Delfi, A. Emendato, D. Ami, D.V. Laurents, A. Natalello, R. Spadaccini, D. Picone, Probing structural changes during amyloid aggregation of the sweet protein MNEI, FEBS J. 287 (2020) 2808–2822. https://doi.org/10.1111/febs.15168.

[23] F. Donnarumma, A. Emendato, S. Leone, C. Ercole, G. D'Errico, D. Picone, Salt Modulated Fibrillar Aggregation of the Sweet Protein MNEI in Aqueous Solution, J Solution Chem. 47 (2018) 939–949. https://doi.org/10.1007/s10953-018-0764-6.

[24] Q. Liu, L. Li, L. Yang, T. Liu, C. Cai, B. Liu, Modification of the Sweetness and Stability of Sweet-Tasting Protein Monellin by Gene Mutation and Protein Engineering, BioMed Research International. 2016 (2016) 1–7. https://doi.org/10.1155/2016/3647173.

[25] V. Esposito, R. Gallucci, D. Picone, G. Saviano, T. Tancredi, P.A. Temussi, The Importance of Electrostatic Potential in The Interaction of Sweet Proteins with the Sweet Taste Receptor, Journal of Molecular Biology. 360 (2006) 448–456. https://doi.org/10.1016/j.jmb.2006.05.020.

[26] M. Delfi, A. Emendato, S. Leone, E.A. Lampitella, P. Porcaro, G. Cardinale, L. Petraccone, D. Picone, A Super Stable Mutant of the Plant Protein Monellin Endowed with Enhanced Sweetness, Life. 11 (2021) 236. https://doi.org/10.3390/life11030236.

[27] Z. Sun, Q. Liu, G. Qu, Y. Feng, M.T. Reetz, Utility of B-Factors in Protein Science: Interpreting Rigidity, Flexibility, and Internal Motion and Engineering Thermostability, Chem. Rev. 119 (2019) 1626–1665. https://doi.org/10.1021/acs.chemrev.8b00290.

[28] V. Esposito, R. Gallucci, D. Picone, G. Saviano, T. Tancredi, P.A. Temussi, The Importance of Electrostatic Potential in The Interaction of Sweet Proteins with the Sweet Taste Receptor, Journal of Molecular Biology. 360 (2006) 448–456. https://doi.org/10.1016/j.jmb.2006.05.020.

[29] W. Zheng, L. Yang, C. Cai, J. Ni, B. Liu, Expression, purification and characterization of a novel double-sites mutant of the single-chain sweet-tasting protein monellin (MNEI) with both improved sweetness and stability, Protein Expression and Purification. 143 (2018) 52–56. https://doi.org/10.1016/j.pep.2017.10.010.

[30] T. Weiffert, S. Linse, Protein stabilization with retained function of monellin using a split GFP system, Sci Rep. 8 (2018) 12763. https://doi.org/10.1038/s41598-018-31177-z.

[31] N. Aghera, I. Dasgupta, J.B. Udgaonkar, A Buried Ionizable Residue Destabilizes the Native State and the Transition State in the Folding of Monellin, Biochemistry. 51 (2012) 9058–9066. https://doi.org/10.1021/bi3008017.

[32] Y. Yoshimura, Y. Lin, H. Yagi, Y.-H. Lee, H. Kitayama, K. Sakurai, M. So, H. Ogi, H. Naiki, Y. Goto, Distinguishing crystal-like amyloid fibrils and glass-like amorphous aggregates from their kinetics of formation, Proc. Natl. Acad. Sci. U.S.A. 109 (2012) 14446–14451. https://doi.org/10.1073/pnas.1208228109.

[33] D.-S. Yang, C.M. Yip, T.H.J. Huang, A. Chakrabartty, P.E. Fraser, Manipulating the Amyloid-β Aggregation Pathway with Chemical Chaperones, Journal of Biological Chemistry. 274 (1999) 32970–32974. https://doi.org/10.1074/jbc.274.46.32970.

[34] P. Arosio, B. Jaquet, H. Wu, M. Morbidelli, On the role of salt type and concentration on the stability behavior of a monoclonal antibody solution, Biophysical Chemistry. 168–169 (2012) 19–27. https://doi.org/10.1016/j.bpc.2012.05.004.

[35] L.A. Sikkink, M. Ramirez-Alvarado, Salts enhance both protein stability and amyloid formation of an immunoglobulin light chain, Biophysical Chemistry. 135 (2008) 25–31. https://doi.org/10.1016/j.bpc.2008.02.019.

[36] A.W. Fitzpatrick, T.P.J. Knowles, C.A. Waudby, M. Vendruscolo, C.M. Dobson, Inversion of the Balance between Hydrophobic and Hydrogen Bonding Interactions in Protein Folding and Aggregation, PLoS Comput Biol. 7 (2011) e1002169. https://doi.org/10.1371/journal.pcbi.1002169.

[37] G. Wei, Z. Su, N.P. Reynolds, P. Arosio, I.W. Hamley, E. Gazit, R. Mezzenga, Self-assembling peptide and protein amyloids: from structure to tailored function in nanotechnology, Chem. Soc. Rev. 46 (2017) 4661–4708. https://doi.org/10.1039/C6CS00542J.

[38] M. Peydayesh, J. Vogt, X. Chen, J. Zhou, F. Donat, M. Bagnani, C.R. Müller, R. Mezzenga, Amyloid-based carbon aerogels for water purification, Chemical Engineering Journal. 449 (2022) 137703. https://doi.org/10.1016/j.cej.2022.137703.

[39] C. Vonrhein, C. Flensburg, P. Keller, A. Sharff, O. Smart, W. Paciorek, T. Womack, G. Bricogne, Data processing and analysis with the autoPROC toolbox, Acta Crystallogr D Biol Crystallogr. 67 (2011) 293–302. https://doi.org/10.1107/S0907444911007773.

[40] G.N. Murshudov, P. Skubák, A.A. Lebedev, N.S. Pannu, R.A. Steiner, R.A. Nicholls, M.D. Winn, F. Long, A.A. Vagin, REFMAC 5 for the refinement of macromolecular crystal structures, Acta Crystallogr D Biol Crystallogr. 67 (2011) 355–367. https://doi.org/10.1107/S0907444911001314.

[41] P. Emsley, B. Lohkamp, W.G. Scott, K. Cowtan, Features and development of Coot, Acta Crystallogr D Biol Crystallogr. 66 (2010) 486–501. https://doi.org/10.1107/S0907444910007493.

[42] D.A. Case, K. Belfon, I.Y. Ben-Shalom, S.R. Brozell, D.S. Cerutti, T.E. Cheatham III, V.W.D. Cruzeiro, T.A. Darden, R.E. Duke, G. Giambasu, M.K. Gilson, H. Gohlke, A.W. Goetz, R. Harris, S. Izadi, S.A. Izmailov, K. Kasavajhala, A. Kovalenko, R. Krasny, T. Kurtzman, T.S. Lee, S. LeGrand, P. Li, C. Lin, J. Liu, T. Luchko, R. Luo, V. Man, K.M. Merz, Y. Miao, O. Mikhailovskii, H. Nguyen, G.M., A. Onufriev, F. Pan, S. Pantano, R. Qi, D.R. Roe, A. Roitberg, C. Sagui, S. Schott-Verdugo, J. Shen, C.L. Simmerling, N.R. Skrynnikov, J. Smith, J. Swails, R.C. Walker, J. Wang, L. Wilson, R.M. Wolf, X. Wu, Y. Xiong, Y. Xue, D.M. York, P.A. Kollman, Amber 2020, University of California, San Francisco, n.d.

[43] R. Anandakrishnan, B. Aguilar, A.V. Onufriev, H++ 3.0: automating pK prediction and the preparation of biomolecular structures for atomistic molecular modeling and simulations, Nucleic Acids Research. 40 (2012) W537–W541. https://doi.org/10.1093/nar/gks375.

[44] D.R. Roe, T.E. Cheatham, PTRAJ and CPPTRAJ: Software for Processing and Analysis of Molecular Dynamics Trajectory Data, J. Chem. Theory Comput. 9 (2013) 3084–3095. https://doi.org/10.1021/ct400341p.

[45] H. Nguyen, D.A. Case, A.S. Rose, NGLview–interactive molecular graphics for Jupyter notebooks, Bioinformatics. 34 (2018) 1241–1242. https://doi.org/10.1093/bioinformatics/btx789.

Declaration of interests

☒The authors declare that they have no known competing financial interests or personal relationships that could have appeared to influence the work reported in this paper.

☐The authors declare the following financial interests/personal relationships which may be considered as potential competing interests: